Journal Name

ARTICLE

Self-healable Fluorescence Active Hydrogel Based On Ionic Block Copolymer Prepared via Ring Opening Polymerization and Xanthate Mediated RAFT Polymerization

Received 00th January 20xx,
Accepted 00th January 20xx

DOI: 10.1039/x0xx00000x

www.rsc.org/

Sovan Lal Banerjee[a], Richard Hoskins[b], Thomas Swift[b], Stephen Rimmer[b*] and Nikhil K. Singha[a*]

In this work we report a facile method to prepare a fluorescence active self-healable hydrogel via incorporation of fluorescence responsive ionic block copolymers (BCPs). Ionic block copolymers were prepared via a combined effect of ring opening polymerization (ROP) of ε-caprolactone and xanthate mediated reversible addition-fragmentation chain transfer (RAFT) polymerization . Here polycaprolactone (PCL) was modified with xanthate to prepare a PCL based macro-RAFT agent and then it was utilized to prepare block copolymers with cationic poly(2-(methacryloyloxy)ethyltrimethyl ammonium chloride) (PCL-*b*-PMTAC) and anionic poly(Sodium 4-vinylbenzenesulfonate) (PCL-*b*-PSS). During the block formation, the cationic segments were randomly copolymerized with trace amount of Flourescein O-acrylate (FA) (acceptor) whereas the anionic segments were randomly copolymerized with trace amount of 9-Anthryl methylmethacrylate (AMMA) (donor) to make both the segments fluorescent. The block copolymers form micelles in DMF:water mixture (1:4 volume ratio). The ionic interaction of two BCPs was monitored via Förster resonance energy transfer (FRET) and zeta potential measurements. The oppositely charged BCPs were incorporated into a polyacrylamide (PAAm) based hydrogel that demonstrated self-healing behavior and is also highly fluorescent.

Introduction

After the invention of the first synthetic hydrogel in 1960 by Lim and Otto[1], they have been extensively used in different biomedical applications e.g. in tissue engineering[2], drug delivery[3], cell culture[4], artificial organ development[5, 6]. The extensive use of the different types of hydrogels in several potential fields is due to their high water content, elasticity, highly porous micro structure and 3D network which resemble biological tissues[7]. Recently fluorescent active hydrogels have been developed for use in several applications due to their optical response[8], which can be utilized in drug delivery systems, glucose sensors[9, 10], thermoresponsive sensors[11], insulin sensors[12], and real time monitoring of the hydrogel behaviour like deformation, movement, degradation, fluorescence guided monitoring of surgery etc[13-17]. Many fluorescent materials such as conjugated conductive polymers[18, 19], fluorescent nanoparticles (i.e Ag NPs)[20, 21], fluorescent organic nanoparticles (FONs)[22], carbon quantum dots (QDs),nanodots[23-25] and fluorescent dyes[26] are used to incorporate luminescent properties in the polymeric hydrogel system. However these materials suffer from several issues including: (i) high probability of aggregation of the nanodots or nano materials, resulting in self-quenching of fluorescence (ii) leaching of the nano materials can cause a toxic effect on the environment and (iii) the low structural stability in the presence of physical and chemical impacts. These issues could be overcome by employing a functional organic polymer consisting of covalently bound fluorophore units[27]. Incorporation of covalently bound fluorescent labels has been shown to be a powerful way of studying both the internal conformational changes of stimuli responsive polymers[28, 29] and the complexation of multiple polymers in solution[30, 31], and FRET analysis using two chromophores can provide additional information in both systems[32, 33]. Recently Ma et. al. reported a protein based hydrogel that can show green and red fluorescence but this system exhibits fluorescence only in the UV range, which hinders their *in vivo* application, and they are of low mechanical strength[17]. Along with the fluorescence properties it will be advantageous for a hydrogel to have self-healing behaviour. Self-healing is a biological phenomenon that provides a spontaneous recovery of the wound without any external stimuli. In synthetic polymeric system self-healing can be of two types; (i) induced self-healing like pH[34], light[35], heat[36] etc. and (ii) non-induced self-healing via formation of ionic interaction[34], H-bonding[37], π-π stacking[38], metal co-ordination[39] etc. Until now reports based on hydrogels having multifunctional ability like self-healing and fluorescent properties are rare. So in this work, our aim is to synthesize tough, self-healable, fluorescent active and non-toxic multifunctional hydrogel. Labelling with fluorescent groups on the different polymers allowed us to use Förster resonance energy transfer (FRET) to study the interactions of the two

[a] *Rubber Technology Centre, Indian Institute of Technology, Kharagpur-721302, India.*
[b] *School of Chemistry and Biosciences, University of Bradford, Bradford, West Yorkshire, BD7 1DP, UK*

Electronic Supplementary Information (ESI) available: Characterization data (NMR, FTIR, Mass Spec, DLS) for compounds in this manuscript. See DOI: 10.1039/x0xx00000x

oppositely charged blocks in aqueous media. The materials were also shown to be non-cyto toxic in cell culture.

In this case we first synthesized oppositely charged block copolymers using polycaprolactone-RAFT (PCL-RAFT) as a macro RAFT agent. PCL-RAFT was synthesized via ring opening polymerization (ROP) of ε-caprolactone (CL) using butanol as a ring opening initiator followed by the modification of the end group to incorporate xanthate functionality. This macro RAFT agent was utilized to prepare positively and negatively charged ionic block copolymers (BCPs). During the formation of ionic block copolymers trace amount of fluorescein O-acrylate (FA) and 9-anthryl methylmethacrylate (AMMA) was copolymerized with cationic and anionic segments respectively to make them fluorescent. The interaction of the BCPs was monitored via Förster resonance energy transfer (FRET) and zeta potential measurement. These two fluorescent active BCPs were incorporated in poly(acrylamide) based hydrogels and the self-healing property of the hydrogel was monitored using mechanical analysis.

Experimental

Materials

ε-caprolactone (CL) (Aldrich, St Louis, USA, 99 %) was dried over calcium hydride (CaH_2) for 48 h at room temperature and then was distilled under reduced pressure. Triethylamine (Et_3N), 2-bromopropionyl bromide (97%) (BiBr), stannous 2-ethylhexanoate [$Sn(Oct)_2$] (99%), 2-(methacryloyloxy)ethyltrimethyl ammonium chloride (MTAC) solution (80% in H_2O) (monomer, purified by passing through basic alumina column), 4-vinyl sodium styrenesulfonate (SS) (monomer), acrylamide (monomer), N,N,N',N'-Tetramethyl ethylenediamine (TEMED) (catalyst), ammonium persulfate (APS) (thermal initiator), 4, 4'- Azobis (4-cyanovaleric acid) (ABCVA) (thermal initiator), N,N'-Methylene bisacrylamide (MBA) (crosslinker), fluorescein O-acrylate (FA), n-Butanol (BuOH), carbon disulfide (CS_2), potassium hydroxide (KOH), diethyl ether (Et_2O), dicholoro methane (CH_2Cl_2, DCM), ethanol (EtOH), sodium hydrogen carbonate ($NaHCO_3$) and anhydrous magnesium sulfate ($MgSO_4$) were purchased from Sigma-Aldrich, USA. 9-Anthryl methylmethacrylate (AMMA) was purchased from TCI chemicals, Japan.

Methods

Synthesis of PCL-OH

In a typical synthesis method ε-caprolactone (32 g, 280.35 mmol) was weighed out and butanol (365 µl, 0.295 g, 4 mmol) was added together with stannous 2-ethylhexanoate ($Sn(Oct)_2$) (256 µl) as a catalyst. The reaction vessel was sealed and purged with nitrogen and heated at 100°C for 3 h. On cooling the polymer solidified and was redissolved in DCM and precipitated out in diethyl ether to obtain the white powder (Yield= 92%). Molecular weight of the polymer was determined from ^{1}H NMR ($M_{n\ NMR}$ = 7800 g mol^{-1}) and GPC ($M_{n\ GPC}$ = 8500 g mol^{-1} ; $Đ$ = 1.30).

Synthesis of PCL-Br

Functionalization of PCL-OH to PCL-Br was performed according to Kuo et al[40]. In a typical synthesis method BiBr (0.56 ml, 2.59 mmol) was added drop-wise to a continuous stirring mixture of PCL-OH (5 g, 0.647 mmol) and triethylamine (0.9 ml, 8.91 mmol) in dry DCM (40 ml) at 0°C for 1 h. After complete addition of the BiBr, the whole reaction mixture was allowed to stir at room temperature for 48 h. After that the reaction mixture was poured into 30 ml of 5% $NaHCO_3$ solution for neutralization of the resultant solution. This process was repeated for 3 times and then the solution was washed with deionized water. The separation of the organic layer was carried out using a separating funnel and the resultant solution was dried over $MgSO_4$. The solution was then filtered and precipitated in diethyl ether for purification. The resulting polymer was separated out via filtration and dried under vacuum for 24 h.

Synthesis of potassium O-ethyl xanthate

2.8 g (50 mmol) of KOH was stirred in 30 mL (0.645 mol) of ethanol until a clear solution was obtained. Then, 10 mL (131 mmol) of CS_2 was added slowly to the above solution under continuous stirring condition and after that the reaction was carried out for 24 h. The obtained reaction mixture was suspended in 300 mL diethyl ether and filtered. The solid product was washed three times with diethyl ether and dried under vacuum at room temperature for 24 h. The purity of the obtained light yellow colored solid was analyzed using the melting point determination (210 °C)[41]. ^{1}H NMR (D_2O, δ = 1.27 ppm (-CH_3) and at δ = 4.40 ppm (-CH_2-)), ^{13}C NMR (D_2O, δ = 13.65 ppm (-CH_3), δ = 70.17 ppm (-CH_2-) and δ = 207.17 ppm (C=S)) and mass spectra (The peak at 198.8 corresponds to the combined weight of the xanthate and potassium).

Synthesis of PCL based macro RAFT agent

In a typical synthesis process, 2 g [0.256 mmol, calculated on the basis of $M_{n\ NMR}$ =7800 g mol^{-1}] of PCL-Br and 0.16 g of potassium O-ethyl xanthate (0.998 mmol) were taken in a nitrogen purged round bottom flask and then degassed by three freeze-pump-thaw cycles. In another dried and nitrogen purged round bottom flask, 0.5 mL (8.5 mmol) of degassed pyridine was dissolved in 10 mL of degassed DCM under continuous stirring condition. The resultant solution was added dropwise to the previously prepared reaction mixture with constant stirring at 0°C and under nitrogen atmosphere. After complete addition, the reaction mixture was allowed to stir at room temperature for 36 h and then diluted with 25 mL of DCM. The solution was washed consecutively with saturated NH_4Cl solution (4×25 mL) and saturated $NaHCO_3$ solution (4×25 mL), and distilled water (4×50 mL). After that the resultant solution was separated out using a separating funnel and the obtained organic layer was dried over anhydrous $MgSO_4$ and

then filtered. The obtained solution was rotary evaporated to get the light yellow coloured PCL based Macro RAFT reagent.

Synthesis of ionic block copolymer (BCP) using PCL based macro-RAFT reagent

In a typical polymerization reaction, PCL-RAFT ($M_{n\ NMR}$ = 7800 g mol^{-1}) (0.3 g, 3.85 X 10^{-2} mmol) was dissolved in 3 ml of DMF in a Schlenk tube. After that the monomer, MTAC (0.5 g, 2.425 mmol) and the initiator, ABCVA (0.0035 g, 3.005 X 10^{-5} mmol) were added into the reaction tube under inert atmosphere. The whole reaction mixture was placed in oil bath kept at 80°C after purging N_2 for 30 min. After 24 h, the obtained reaction mixture was placed in an ice bath and opened to air to stop the reaction. It was then precipitated in diethyl ether. After that, the obtained precipitate was again dissolved in DMF and was dialysed in deionized water to remove the unreacted monomers and other reagents. Dialysis tube having a molecular weight cut off of 3500 Da was used for dialysis. Finally the BCP, PCL-*b*-PMTAC was freeze dried to get the final product. A Similar procedure was adopted to get the PCL-*b*-PSS. ^{1}H NMR was utilized to determine the conversion of polymerization reaction. To determine the interaction between the BCPs, the cationic block copolymer was copolymerized with FA (0.5% of monomer amount, acceptor) (FAPCL-*b*-PMTAC) whereas the anionic block copolymer was copolymerized with 9-AMMA (0.5% of monomer amount, donor) (AMMAPCL-*b*-PSS).

Synthesis of oppositely charged BCP micelle encapsulated polyacrylamide based hydrogel

In a typical synthesis process 10 mL (concentration 10 mg mL^{-1}) of fluorescent cationic BCP micelle mixed with 10 mL of fluorescent anionic BCP micelle under vigorous stirring condition in a 3 neck round bottom flask and homogenized for 1 h under inert atmosphere. After that 7 mL of 20 wt% aqueous solution of acrylamide, 2 mL of 1 wt% aqueous solution of crosslinker (MBA) and initiator (APS) were added into the BCPs solution sequentially under inert atmosphere and allowed to stir for another 15 min for proper homogenization. After that 2 wt% aqueous solution of TEMED was injected into the mixture and was stirred for 5 min. Then the solution was transferred into a rectangular mould having a dimension of 40 mm x 15 mm x 3 mm (L x W x T) to get a perfectly shaped micelles containing fluorescent hydrogel. The mixture was allowed to gel for 24 h and then the rectangular shaped hydrogel was dipped into ethanol water mixture (1:4 volume ratios) for 16 h to make the hydrogel free from unreacted monomer and DMF. After that the hydrogel was taken out from the solution and allowed to dry in a vacuum oven at 50°C for 48 h. Polyacrylamide based hydrogel having no BCPs and hydrogel consists of only cationic and anionic BCP micelle were also prepared as a control sample. Details of the synthesis formulation are summarized in Table 1.

Characterisation

Fourier transform infrared spectroscopy (FTIR) (Perkin Elmer, model spectrum-2) was utilized to characterize the prepared sample. FTIR was operated in an ATR mode and at a scanning range of 500-4000 cm^{-1}. Diffusion ordered NMR spectroscopy (DOSY spectra) and proton nuclear magnetic resonance (^{1}H NMR) spectra were recorded on a Bruker Avance III 400-MHz spectrometer at room temperature (25 ± 1°C) using D_2O as solvent.

Table 1. Summary of hydrogel formation [*#$+^]

Batch	Cationic micelle[a]	Anionic micelle[a]
S1	2 ml ($FAPCL_{70}$-b-$PMTAC_{48}$)	2 ml ($AMMAPCL_{70}$-b-PSS_{48})
S2	2 ml ($FAPCL_{70}$-b-$PMTAC_{97}$)	2 ml ($AMMAPCL_{70}$-b-PSS_{97})
S3	2 ml ($FAPCL_{70}$-b-$PMTAC_{48}$)	X
S4	X	2 ml ($AMMAPCL_{70}$-b-PSS_{48})
S5	2 ml ($FAPCL_{70}$-b-$PMTAC_{97}$)	X
S6	X	2 ml ($AMMAPCL_{70}$-b-PSS_{97})
S7	X	X

[*] Amount of acrylamide = 4 g [Total monomer concentration = 20 wt%], [#] Amount of MBA = 0.04 g [1 wt% of monomer amount], [$] Amount of APS = 0.04 g [1 wt% of monomer amount], [^] Amount of TEMED = 0.08 g [2 wt% of monomer amount], [+] Total batch volume = 20 ml [a] (Conc. = 4mg/ml in 1:4 DMF :water mixture)

In case of DOSY analysis the gradient strength was gradually increased from 2% to 95% in a sequence of 16 steps. Bipolar rectangular gradients were maintained for duration of 2 ms and the gradient recovery delay was 200 ms. A maximum of 0.535 T m^{-1} gradient strength was used and the diffusion time was recorded in between 0.5 s and 1.0 s. The obtained spectrum was analysed using Topspin 2.1.6 software (Bruker). Molar mass and polydispersity (*Đ*) was determined using gel permeation chromatography (GPC) (Viscotek Gel Permeation Chromatograph equipped with a VE 1122 solvent delivery system, narrow dispersed polystyrene used as a standard) analysis at room temperature. Tetrahydrofuran (THF) was used as an eluent at a flow rate of 1mL min^{-1} and the data was analysed using OmniSEC 4.2 software. Field emission scanning electron microscopy (ZEISS, FESEM) operated at an accelerating voltage of 5kV was used to analyse the surface morphology of the prepared samples. To analyse the BCP micelle, the dilute solution (1mg/mL) (DMF:Water = 1:4 volume ratio) of BCPs was spin coated over glass slide and allowed to dry at 40°C inside vacuum oven. To analyse the solid gel sample the dried hydrogel was stuck over the stab using carbon adhesive tape. Before taking the images all the samples were gold coated. To examine the bulk morphology of micelles, Transmission electron microscopy (TEM) (JEOL, JEM-2000E7) was used. Dilute solution of micelles (1 mg mL^{-1}) (DMF:Water = 1:4 volume ratio) was drop cast over a carbon coated TEM grid having 300 mesh size and dried at ambient temperature before imaging. Atomic force microscopy (AFM) (Agilent 5500, USA) was also used to analyse the surface morphology of the micelle. Samples were prepared using the same process as used for FESEM analysis. Tapping mode was used during AFM analysis. X-ray diffraction analysis (XRD) was

carried out (PANalytical, Netherlands) using Copper X-ray source (1.549 Å) with standard angle of 0-80 degree (2θ) and at a fixed scan rate of 1˚ per minutes. Dynamic light scattering (DLS) instrument (Malvern Nano ZS) was used to analyse the particle size of the BCPs. A scattering angle of 90° and a He-Ne (4 mW, λ = 632.8 nm) laser was used for this experiment. Water contact angles (WCA) of synthesized polymers were obtained at ambient temperature using a Rame-Hart 260 F4 standard Goniometer. A drop of liquid was placed onto the surface of the polymer film and the contact angles were measured within 5-10 Sec. Fluorescence measurements were carried out on a Horiba Fluoromax-4 Luminescence Spectrometer with a Xenon discharge lamp and Monk-Gillieson type monochromators. The monochromator has a wavelength accuracy of ± 1.0 nm. Emission and excitation slit width were maintained at 1 nm. The excitation scans were carried out by taking a fixed emission wavelength of 365 nm and 475 nm for AMMA and FA tagged BCPs respectively. For the FA labelled BCP, the excitation wavelength of 480-800 nm and for the AMMA labelled BCP, the excitation wavelength of 370-720 nm was fixed during the experiments. Tensile test analysis was carried out to confirm the self-healing ability of the hydrogel. Tensile testing was carried out in Hounsfield H10KS tensile test machine by maintaining a crosshead speed of 10 mm/min and a load cell of 500 N at room temperature. During the tensile experiment the hydrogel samples were coated with silicon oil to prevent the elimination of entrapped water. Thermal properties of the block copolymer were analysed using differential scanning calorimetric analysis (DSC) (DSC 200 F3 instrument (Netzsch, Germany). The samples were heated from -100°C to 200°C under nitrogen atmosphere at a heating rate of 20°C/min. The temperature against the heat flow was recorded.

Swelling study of the synthesized hydrogel

The swelling ratio of the prepared hydrogel was determined gravimetrically. To study the swelling behaviour of the individual hydrogels, a preweighed amount of cylindrical shaped hydrogel sample was dipped into the PBS buffer solution having a pH of 7.4. After a certain time interval swollen hydrogel was taken out from the solution and the surface water was removed by gently pressing the hydrogel with tissue paper before weighed. The swelling ratio was calculated using the following formula-

$$Q = \frac{W_{swell} - W_{dry}}{W_{dry}}$$

Where, W_{swell} and W_{dry} are the swollen weight and dry weight of the hydrogel sample respectively.

Dynamic Mechanical Analysis (DMA)

Creep study

Creep compliance measurements were carried out using a Dynamic Mechanical Analyzer (DMA), Metravib 50 N, France. The creep experiment was performed in the tension mode. For this experiment, the hydrogel samples (as prepared and self-healed) were subjected to a constant stress of 0.1 MPa. The resulting strain and its recovery were recorded at 25°C. The creep compliance D(t) was calculated from the obtained stress and strain data using the following equation-

$$Creep = D(t) = \frac{\varepsilon(t)}{\sigma_0}$$

Where, σ_0 and $\varepsilon(t)$ are respectively stress and strain on the samples.

Stress relaxation study

Stress relaxation experiments were also performed in the tension mode of the DMA instrument at 25°C. The samples were subjected to a constant strain of 0.02%, and the resulting stress and its recovery were monitored. The as obtained stress and strain data were used to calculate the relaxation modulus E(t) using the following equation-

$$Stress\ relaxation = E(t) = \frac{\sigma_t(t)}{\varepsilon_0}$$

where, $\sigma_t(t)$ and ε_0 are respectively stress and strain on the sample.

In-vitro cell cytotoxicity Assay:

NIH 3T3 cell line was used to study the *in-vitro* cell cytotoxicity assay. Here the MTT (3-(4,5-dimethylthiazol-2-yl)-2,5-diphenyltetrazolium bromide) colorimetric technique was adopted to monitor the change in the metabolic activity of the fibroblast cell in the presence of the hydrogel. During the analysis a purple colored formazan salt was formed and by measuring the O.D. value at 590 nm one can identify the amount of cell viability. At definite cell condition the oxidoreductase enzymes reduced the MTT salt to generate formazan salt. Fibroblast cells at a concentration of 1 X 10^4 cells per well were seeded in 96-well plate using 180 µl of DMEM medium containing 10% FBS and 1% antibiotic. Then the PBS buffer containing hydrogel suspension was added to the medium and it was allowed to culture for 48 h in humidified atmosphere in presence of 5% CO_2. Cells in growing medium containing no hydrogel were taken as a positive control. After that the culture was washed with PBS solution and MTT solution having a concentration of 1 mg mL^{-1} was added before incubation for 4 h at 37°C. After the incubation the supernatant was removed and insoluble formazan salt was dissolved in DMSO. The O.D. value of the purple solution was taken at a wavelength of 590 nm. The relative cell viability was calculated using the following equation-

$$\text{Cell viability } (\%) = \frac{\text{O.D. }_{590\ (\text{sample})}}{\text{O.D.}_{590\ (\text{control})}}$$

Statistical analysis:

All the experiments of tensile testing and the *in vitro* cell cytotoxicity assay were carried out in triplicates and the reported values are the average of all triplicates value ±

standard deviation. The student's t-test was used to compare the statistical significance of test samples against control.

Results and Discussion

Cationic (PCL-*b*-PMTAC) and the anionic (PCL-b-PSS) amphiphilic block copolymers (BCPs) with different block length of cationic and anionic segments were prepared using PCL-RAFT as a macro RAFT agent. The PCL based macro RAFT agent was synthesized via a successive ROP of ε-caprolactone (CL) and xanthation of the prepared PCL unit. ROP of ε-caprolactone was carried out using butanol as a ring opening initiator and stannous 2-ethylhexanoate [$Sn(Oct)_2$] as a catalyst. The molecular weight of the PCL was determined from the ^{1}H NMR (M_n = 7800 g mol^{-1}) and GPC analyses (M_n = 8500 g mol^{-1}, $Đ$ = 1.30). During the molecular weight calculation by ^{1}H NMR, the characteristic peaks of PCL at δ = 0.98 ppm (a, -CH_3 proton) and at δ = 2.4 ppm (e, -CO-C**H$_2$**) were considered (Figure 1(i)). The PCL was further utilized to prepare the macro-RAFT agent. To prepare the macro-RAFT agent, PCL was initially treated with BiBr and after that the obtained product was reacted with potassium O-ethyl xanthate. The successful bromination and xanthation of PCL unit was verified from ^{1}H NMR analysis. For the PCL-Br the characteristic peak appeared at δ = 1.9 ppm (**k**, -CH-C**H$_3$**) and at δ = 4.4 ppm (**j**, -CO-C**H**) (Figure 1(ii)). After xanthation a new resonance appeared at δ = 4.7 ppm (l, CS-O-C**H$_2$**) (Figure 1(iii)). Scheme 1 summarizes the preparation of PCL-OH, PCL-Br and PCL based macro-RAFT. For xanthation reaction O-ethyl xanthate was prepared using a previous report and the purity of the sample was checked by determining the melting point of the light yellow coloured solid (m.p. = 210°C), ^{1}H NMR, ^{13}C NMR and mass spec analyses. ^{1}H NMR (Figure S1) analysis of potassium O-ethyl xanthate provides characteristic peaks at δ = 1.27 ppm (-C**H$_3$**) and at δ = 4.40 ppm (-C**H$_2$**-). ^{13}C NMR analysis of potassium O-ethyl xanthate provides characteristic peaks at δ = 13.65 ppm (-**C**H$_3$), δ = 70.17 ppm (-**CH$_2$**-) and δ = 207.17 ppm (C=S). Purity of the prepared xanthate was also checked with the mass spectra analysis. The major peaks obtained are 95, 198.8, 258.8, 518.8 and 678.8. The peak at 198.8 corresponds to the combined weight of the xanthate and potassium. The higher peaks might appear due to the presence of dimers etc.

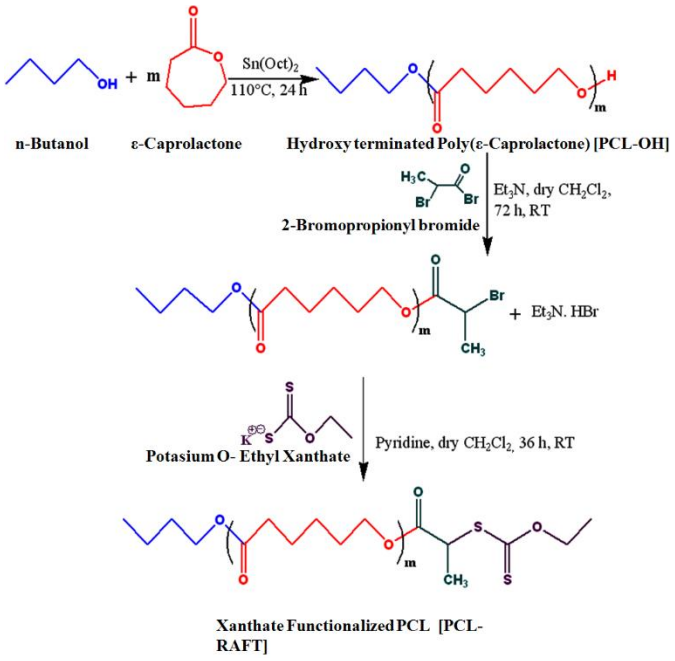

Scheme 1 Synthesis of PCL based macroinitiator and macro-RAFT.

Table 2. Summary of the preparation of poly(caprolactone) (PCL) and its ionic BCP prepared via RAFT polymerization

Sample	Composition	[M]:CTA-RAFT: [I]	Conv. (%)	Target MW (g mol^{-1})	M_n[a] (g mol^{-1})	PCL (mol %)
PCL	PCL_{70}	-	92	8000	7800	100
$PCLPM_1$	PCL_{70}-*b*-$PMTAC_{48}$	50 : 1 : 0.25	97	17936	17559	59
$PCLPM_2$	PCL_{70}-*b*-$PMTAC_{97}$	100 : 1 : 0.25	92	28079	27215	41
$PCLPM_3$	PCL_{70}-*b*-$PMTAC_{194}$	200 : 1 : 0.25	90	48158	46839	26
$PCLPS_1$	PCL_{70}-*b*-PSS_{48}	50 : 1 : 0.25	92	17888	17295	59
$PCLPS_2$	PCL_{70}-*b*-PSS_{97}	100 : 1 : 0.25	88	27982	26327	42
$PCLPS_3$	PCL_{70}-*b*-PSS_{194}	200 : 1 : 0.25	89	47964	44528	26

[a] Molecular weight was determined using ^{1}H NMR.

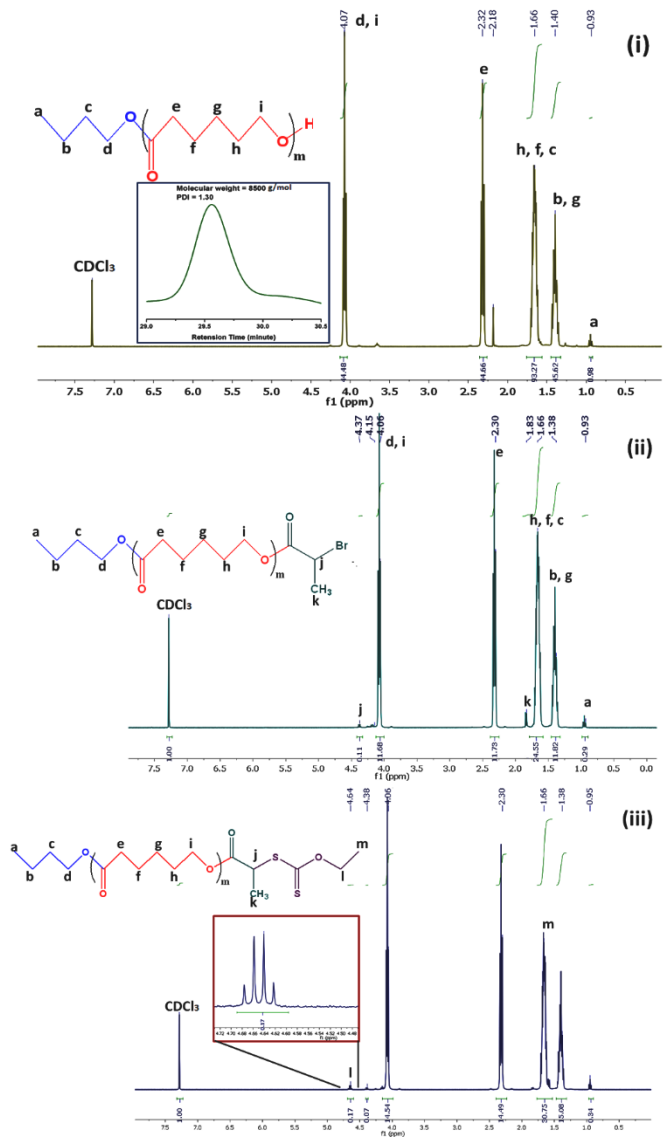

Figure 1 ^{1}H NMR analysis of (i) PCL_{70}-OH formed via ROP, (ii) PCL_{70}-Br and (iii) PCL_{70}-RAFT.

The macro RAFT agent was utilized to prepare the ionic block copolymers via xanthate mediated RAFT polymerization. Both the cationic and anionic block copolymers of different block length were prepared. The Formed BCPs was analysed using ^{1}H NMR analysis and differential scanning calorimetric (DSC) analysis. The summery of the BCPs formation was mentioned in Table-2. The BCPs were prepared using DMF as a solvent and the NMR was conducted using a mixture (1:1 volume ratio) of D_2O and d_8-THF. Schematic representation of the preparation method of fluorescent tagged BCPs is summarized in Scheme 2. The molecular weight of the 2nd ionic block copolymers was determined from ^{1}H NMR analysis. For the PCL_{70}-*b*-$PMTAC_{48}$ (Figure 2(i)) molecular weight of the PMTAC unit was calculated by considering the characteristic peak of PMTAC at δ = 3.21 ppm (**n**, -R-N($C\mathbf{H_3}$)$_3^+$) and characteristic peak of PCL at δ = 2.4 ppm (**e**, -CO-$C\mathbf{H_2}$). Comparing the integral area of these two, the molecular weight of the ionic block was determined and it was 11,270 g mol^{-1}. The same method was applied for the anionic unit PCL_{70}-*b*-PSS_{48} (Figure 2(ii)). By comparing the integral area of the characteristic peak of PSS unit (δ = 7.76 ppm (**0**, Ph-C**H**)) and characteristic peak of PCL at δ = 2.4 ppm (**e**, -CO-$C\mathbf{H_2}$) the molecular weight of the PSS unit was 12,350 g mol^{-1}. To confirm the BCP formation we carried out DOSY analysis which gives the shift of protons in polymer solution and can be used to obtain hydrodynamic radii of polymer systems[42]. This technique was used to demonstrate efficient grafting and the block copolymerization by producing a 2D correlation diagram of chemical shifts on the horizontal axis and the diffusion coefficient in the vertical axis. From the DOSY analysis (Figure 2(iii)a, Figure 2(iii)b and Figure 2(iii)c) it was observed that the distribution of diffusion coefficients of BCP of PCL with the cationic segment (Figure 2(iii)b) and anionic segments (Figure 2(iii)c) were substantially different to that of pristine PCL (Figure 2(iii)a). This indicates that both blocks are attached and diffuse as a single distribution of chains.

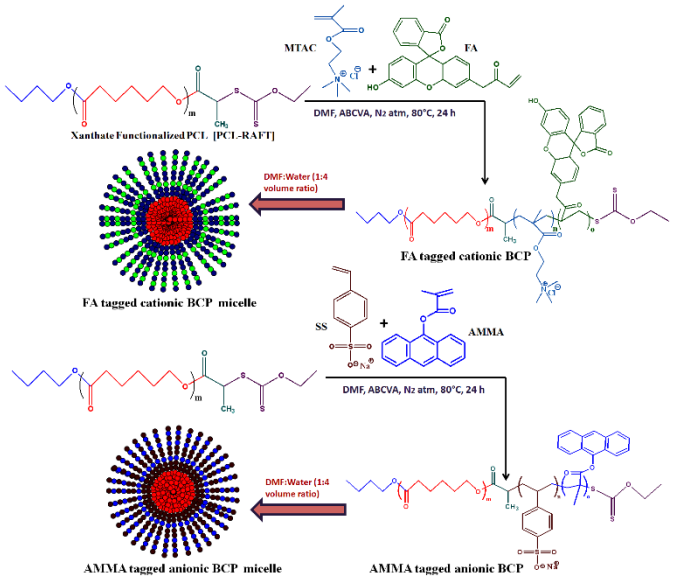

Scheme 2 Synthesis of amphiphilic cationic (PCL-*b*-PMTAC) and anionic (PCL-*b*-PSS) diblock copolymer via ROP and xanthate mediated RAFT polymerization and their self-assembly in DMF: water mixture.

Journal Name

ARTICLE

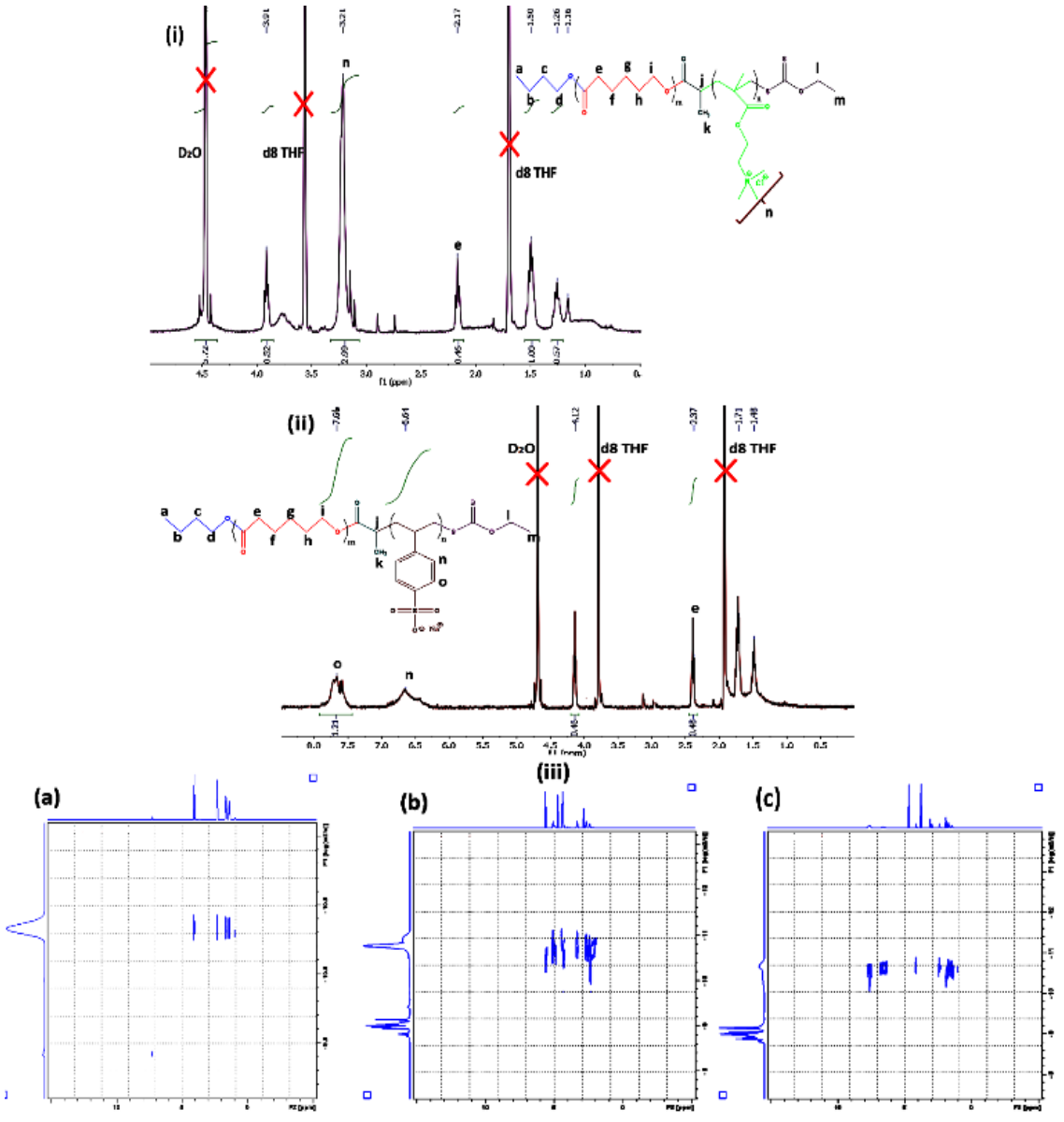

Figure 2 ^{1}H NMR analysis of (i) PCL_{70}-*b*-$PMTAC_{48}$, (ii) PCL_{70}-*b*-PSS_{48}. (iii) DOSY analysis of (a) PCL_{70} (b) PCL_{70}-*b*-$PMTAC_{48}$ and (c) PCL_{70}-*b*-PSS_{48}.

The amphiphilic BCP was further analysed by FTIR analysis. From the Figure S4(a) it was observed that pristine PCL had characteristic absorption bands at 1722 cm^{-1} and 1180 cm^{-1} due to the presence of >C=O stretching and C-O-C stretching respectively. In case of cationic BCP along with the vibrational peaks of PCL new peaks appeared at 1491 cm^{-1} and 942 cm^{-1} which were due to the presence of $-CH_3$ bending vibration of $[RN(CH_3)_3]^+$ and $-CH_3$ stretching vibration of $[RN(CH_3)_3]^+$ respectively.

Presence of PSS unit in the BCP was confirmed by observing the presence of vibrational peaks at 1186 cm^{-1} and 1042 cm^{-1} which are due to anti-symmetric and symmetric vibrational peaks of SO_3^- group.

The change in crystallinity of the PCL unit after the formation of the cationic and anionic BCPs was monitored through XRD analysis. PCL homopolymer shows sharp crystalline peaks at 21° and 24°, which are due to scattering from the [110] and [200] crystallographic planes. Figure S4(b) designates that upon formation of the BCPs the crystalline component of the PCL was reduced and the peak become broader indicating introduction of amorphous characteristics in the BCP[43].

Self-assembly of the ionic amphiphilic BCPs in water: DMF mixture

It is widely reported that BCPs with chemically distinct and immiscible segments combine to form immiscible self-assembled structures when they are dissolved in a solvent with different solubility for different blocks. The morphology of self-assembly depends on a number of factors[44]. When the soluble block has dominancy over the insoluble block it forms a spherical core shell type of structure. In our case the PCL based amphiphilic ionic BCPs form spherical morphology in DMF:water mixtures (1:4 volume ratio). To prepare the core-shell type morphology, initially the cationic and anionic BCPs were dissolved separately in DMF which is a thermodynamically favourable solvent for both of the segments. After homogenization the mentioned amount of the water was added dropwise into the solution with continuous stirring, it was observed that in both cases the opaque BCP dispersion turned relatively transparent, indicating the formation of stable micelles. The formation of stable micellar structures depends on two factors- (i) formation of the stable aggregates by the insoluble part of the BCP and (ii) the repulsive and attractive forces present between the nearby polymer segments and between the polymer-solvent respectively[45]. The morphology of the formed "core-shell" BCPs was observed by using different microscopic techniques like FESEM, HRTEM and AFM analyses and also by DLS study. Light scattering analysis (Figure S5(a)) was utilized to monitor the hydrodynamic radius provided by the different BCPs having different block length of cationic and anionic segments. It was observed that with an increase in the block length of the cationic segment from PCL_{70}-b-$PMTAC_{48}$ to PCL_{70}-*b*-$PMTAC_{97}$ to PCL_{70}-*b*-$PMTAC_{194}$ the hydrodynamic radius also increased gradually from 370 ± 5 nm (Poly dispersity index (PDI) = 0.247) to 440 ± 5 nm (PDI= 0.348). The same phenomenon was also observed in case of anionic segment when the anionic block length was varied from PCL_{70}-b-PSS_{48} to PCL_{70}-*b*-PSS_{97} to PCL_{70}-*b*-PSS_{194} the hydrodynamic radius gradually increased from 325 ± 4 nm (PDI= 0.174) to 348 ± 5 nm (PDI= 0.298). This might be due to the greater solvation of the hydrophilic segments. Interestingly, it was observed that very high block length of cationic and anionic segments hinder the formation of micellar structure and no particle diameter was found. During the dynamic light scattering measurement a solution concentration of 1 mg mL^{-1} was maintained. From the water contact angle (WCA) analysis (Figure S5(b)), it was observed that the formation of the BCP results in a decrease in the WCA. For pristine PCL, the WCA value was 72° whereas the cationic and anionic BCPs showed a WCA value of 32° and 36° respectively. The formation of the ionic BCP aggregates further reduced the WCA value and it was 20° which indicate the hydrophilicity of the assembled complex.

For all the microscopic analysis BCP with poly(ionic) segments of M_n 10 kg mol^{-1} were considered as they have lower micellar size. Figure 3(i) summarizes the microscopic images obtained in FESEM analysis. From the figure it was observed that both the cationic (Figure 3(i)a) and the anionic BCP (Figure 3(i)b) formed spherical micelles. When both the BCPs were mixed together they formed an aggregate, as observed in the FESEM image (Figure 3(i)c). Similar observation was also obtained in HRTEM analysis. From HRTEM study it was observed that the PCL based BCPs formed spherical "core-shell" morphology, where the PCL segment formed the dark core part and the lighter dark corona was formed by the PMTAC (Figure 3(ii)a) and PSS (Figure 3(ii)b) unit in the cationic and anionic BCP respectively. The size obtained from the HRTEM analysis for both of the BCP is in the range of 200 ± 10 nm. It was observed that when both of the oppositely charged BCPs were mixed at a lower concentration the obtained HRTEM image showed a similarity to a worm like morphology. This might be due to the formation of a continuous structure by the ionic interaction between the cationic and the anionic BCPs.

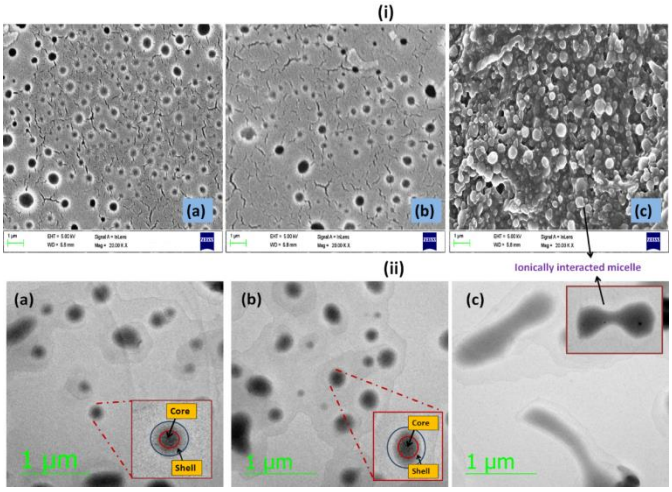

Figure 3 (i) FESEM and (ii) TEM images of the formed - (a) PCL70-b-PMTAC47 micelle, (b) PCL70-b-PSS47 micelle, (c) Ionically interacted BCPs in aqueous solution (picture taken after drying of the solution).

The obtained AFM (Figure 4) images also corroborate the result obtained from FESEM and HRTEM analyses. From the AFM image it was observed that both the cationic (Figure 4a) and anionic (Figure 4b) segments exhibit spherical morphology having "core-shell" structure. The average size obtained for both of the BCPs was in the range of 180 ± 10 nm. The mixture of the two polyelectrolyte BCPs results in aggregated structures (Figure 4c) as obtained in FESEM and HRTEM.

The interaction between the oppositely charged BCPs was further confirmed through additional fluorescence spectroscopy and zeta potential analyses.

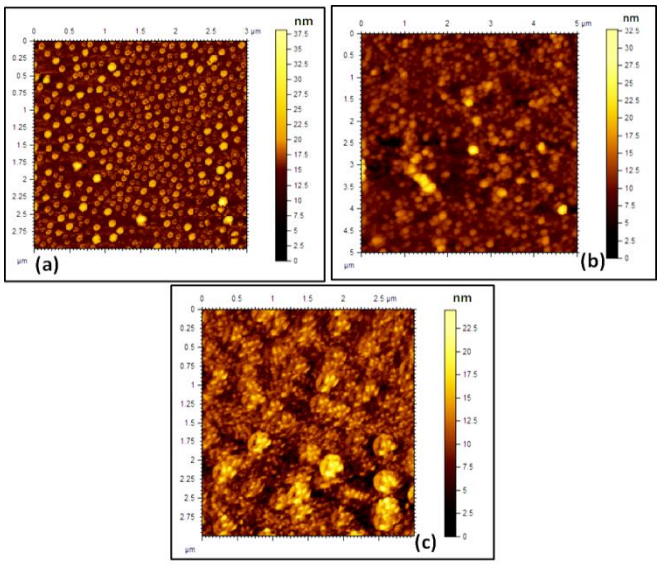

Figure 4: AFM images of the formed - (a) PCL70-b-PMTAC48 micelle, (b) PCL70-b-PSS48 micelle, (c) Ionically interacted BCP micelle in aqueous solution (picture has been taken after drying of the solvent).

To measure the fluorescence activity of the positively and negatively charged BCP, during the block copolymerization of cationic and anionic segments with the PCL unit a small amount (0.5% of the monomer) of fluorescein O-acrylate (FA) (acceptor) and 9-anthryl methylmethacrylate (AMMA) (donor) was copolymerized with PMTAC and PSS unit respectively. Fluorescence excitation scans were carried out by sample excitation at 365 nm and 475 nm for AMMA and FA tagged BCPs respectively in dilute solution. Figure 5a and Figure 5b show the fluorescence emission graph of FA labelled PCL_{70}-*b*-$PMTAC_{48}$ and AMMA tagged PCL_{70}-*b*-PSS_{48} respectively. Additional measurements were carried out and energy transfer between the two chromophores via a FRET mechanism was observed when the cationic and anionic polymers were mixed. In this study 200 µL of AMMA tagged PCL_{70}-*b*-PSS_{48} solution (DMF:Water = 1:4 volume ratio) (Conc. = 10 mg mL^{-1}) was mixed with different volumes of FA tagged PCL_{70}-*b*-$PMTAC_{48}$ solution and the total volume of the solution was maintained at 1 mL. As a result of increasing concentration of FA (acceptor), the intensity of the AMMA (donor) decreased as shown in Figure 5c. This demonstrates the increasing interaction between cationic and anionic segments bringing the two labels together. However, after a certain amount of acceptor containing cationic polymer, equilibrium was achieved and the I_A/I_D value stabilized, indicating a FRET neutralization point (300 µL of cationic BCP added to 200 µL of anionic BCP). After this value no additional FRET occurred with increasing cationic polymer addition. Figure 5g represents the schematic of the FRET between cationic and anionic BCP. As FRET will only occur over a limited spatial distance this measurement indicates the critical ratio of anionic and cationic polymers required to achieve full complexation between the two polymers, and further increases in concentration do not lead to further supramolecular assembly.

The interaction of the oppositely charged micelles is also monitored by studying the variation of the zeta potential value upon addition of the one component (FA tagged PCL_{70}-*b*-$PMTAC_{48}$ solution, positively charged) into another (AMMA tagged PCL_{70}-*b*-PSS_{48} solution, negatively charged). The obtained result is summarized in Table 3. As observed from the result that a gradual increase in the Zeta potential occurs upon addition of the positively charged micellar solution into the negatively charged micellar solution.

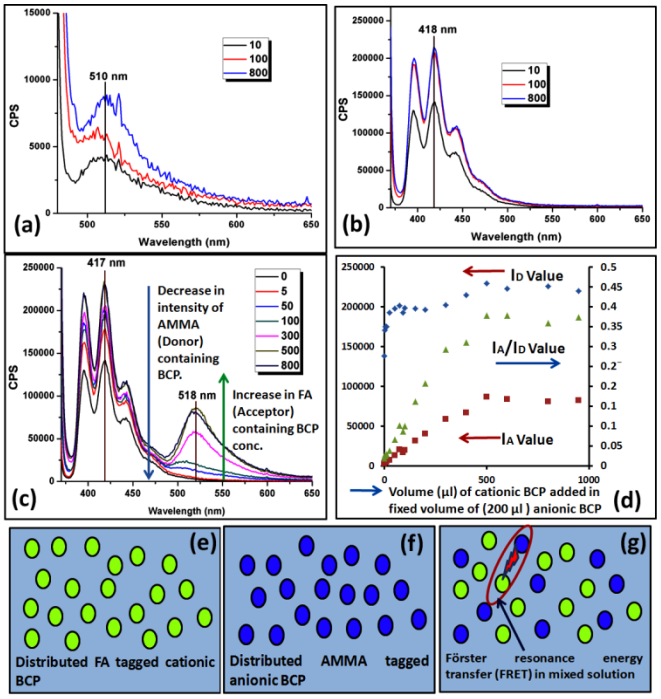

Figure 5 Fluorescence spectroscopic results of (a) PCL_{70}-b-$PMTAC_{48}$ micelle, (b) PCL_{70}-b-PSS_{48} micelle, (c) results of FRET energy transfer during the mixing of the cationic and anionic BCPs, (d) correlation plot of the FRET when cationic and anionic micelle were mixed together and respective IA/ID plot. Schematic representation of solvent distributed (e) cationic BCP, (f) anionic BCP and (g) FRET between cationic and anionic BCPs.

The concentration of the prepared FAPCL_{70}-*b*-$PMTAC_{48}$ and AMMA PCL_{70}–*b*-PSS_{48} was 10 mg mL^{-1}. Interestingly, it was observed that a transition point appeared during the zeta potential titration when the system suddenly showed a high positively charge value from a high negative charge value. The mid-point of these two transition designates the charge neutrality point. The condition at which charge neutrality achieved is highlighted in the Table 3.

Table 3 Results of zeta potential analysis and FRET analysis when two oppositely charged micelles were mixed together.

Water: DMF mixture (4:1 volume ratio) (µl)	Amount of AMMA tagged PCL_{70}-*b*-$PMTAC_{48}$ solution (µL)*	Zeta Potential (mV)	I_A/I_D value acquired from FRET analysis
798	2	-44.3 ± 2.0	0.0283
795	5	-39.1 ± 2.0	0.0246
790	10	-37.2 ± 1.0	0.0293
775	25	-34.5 ± 2.0	0.0382
750	50	-31.9 ± 2.0	0.0666
720	75	-31.5 ± 1.0	0.1012
710	90	-30.8 ± 1.2	0.0865
700	100	-30.1 ± 1.0	0.1006
650	150	-28.7 ± 2.0	0.1617
600	200	+1.56 ± 2.0	0.2076
500	300	+17.2 ± 1.0	0.2926
400	400	+19.2 ± 1.0	0.3104
300	500	+22.5 ± 2.0	0.3781
200	600	+27.4 ± 2.0	0.3782
0	800	+32.5 ± 3.0	0.3597
0	950	+41.2 ± 3.0	0.3736

Amount of Amount of AMMA tagged PCL_{70}-b-PSS_{48} solution = 200 µl
* Base solvent was prepared by mixing Water:DMF in 4:1 volume ratio.

Thermal Analysis

Thermal analysis of the PCL homopolymer and the PCL based ionic block copolymers were carried out to determine the change in the thermal behaviour of the PCL upon block copolymerization and also to determine the T_g of the segments. It is well known that PCL is a crystalline polymer, so a strong melting point peak appeared at 60°C as shown in Figure 6a. After copolymerization it was observed that the peak intensity was drastically reduced due to the disruption of the crystalline nature of the PCL unit (Figure 6b)[46]. The T_g of the cationic and the anionic segment was determined from the DSC thermogram. Figure 6c and Figure 6d showed that the T_g of the PMTAC and the PSS unit are 35°C and 92°C respectively.

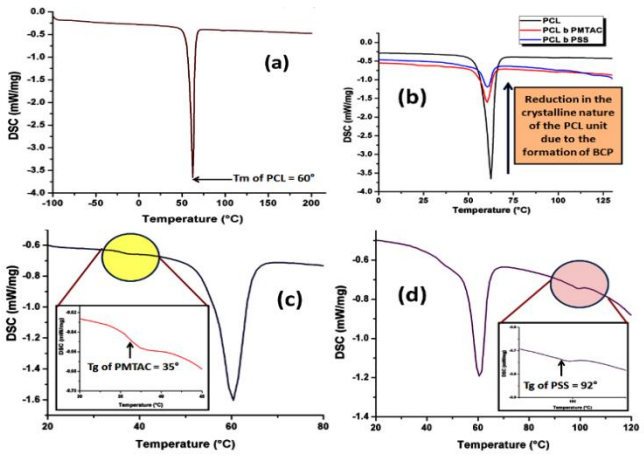

Figure 6 DSC analysis of **(a)** PCL-OH, **(b)** reduction in intensity of the endotherm of PCL upon block copolymer formation, **(c)** PCL_{70}-*b*-$PMTAC_{48}$ and **(d)** PCL_{70}-*b*-PSS_{48}.

Preparation of fluorescence active hydrogel and its swelling properties

As discussed in the experimental section, both the BCP micelle (cationic and anionic) prepared in 1:4 volume ratio of DMF:Water mixture was incorporated in the poly(acrylamide) based hydrogel. Hydrogel was prepared using acrylamide as monomer, MBA as crosslinker and APS as a thermal initiator. TEMED was used as a room temperature gelator. As shown in Figure 7(i), the cationic (Figure 7(i)b) and the anionic (Figure 7(i)c) BCPs were fluorescent and they provided a yellow and a blue colour emission under fluorescence light respectively. The mixture of DMF:Water (1:4 volume ratio) was used as a control sample under fluorescence (Figure 7(i)a). When both of the micelles were mixed with an almost equal charge ratio, it resulted in a mixed colour where the intensity of the yellow and the blue colour was quenched to some extent. This mixture was further used to prepare the fluorescence active hydrogel. Figure 7(i)e and Figure 7(i)f provide the images of the fluorescent hydrogel under visible and fluorescence light. To measure the extent of swelling of the synthesized hydrogel at pH = 7.4 buffer solution, each of the hydrogel was immersed in the buffer solution separately and after a predetermined time interval the swelling ratio was measured gravimetrically. It was observed that with increase in the block length of the incorporated BCP the extent of the swelling was reduced. As observed in the Figure 7(ii), non-modified hydrogel (no BCP incorporation) showed a (1300 ± 26)% swelling whereas hydrogel with $FAPCL_{70}$-*b*-$PMTAC_{48}$ + $AMMAPCL_{70}$–*b*-PSS_{48} showed a (1200 ± 30)% swelling compared to the $FAPCL_{70}$-*b*-$PMTAC_{97}$ + $AMMAPCL_{70}$–*b*-PSS_{97} incorporated hydrogel ((1000 ± 22)% swelling). The deviation in swelling can be explained by considering the ionic interlocking of the BCPs inside the hydrogel. Non-modified hydrogel has no such ionic interaction in the bulk so the free volume is comparatively higher compared to the ionic BCP incorporated hydrogel which results in a higher degree of swelling. In the case of $FAPCL_{70}$-*b*-$PMTAC_{48}$ + $AMMAPCL_{70}$–*b*-PSS_{48} containing hydrogel the ionic block length is comparatively low compared to $FAPCL_{70}$-*b*-$PMTAC_{97}$ + $AMMAPCL_{70}$–*b*-PSS_{97}. It provides a higher degree of swelling as the extent of physical crosslinking (ionic interaction between two oppositely charged BCPs) is less. So as a result the inter crosslinking volume is high which results in a higher extent of swelling.

Mechanical analysis of the hydrogel

As mentioned in the swelling experiment the incorporation of the ionic BCP generates ionic crosslinking inside the hydrogel which results in a lower degree of swelling compared to the non-modified hydrogel sample. The formation of the ionic crosslinking also has an effect over the transparency of the hydrogel. As shown in the Figure 8a the incorporation of BCPs, reduces the transparency of the hydrogel which provides support to the idea that the formation of the ionic crosslinking inside the hydrogel affects transparency. The results obtained from the tensile study are summarized in Figured 8b.

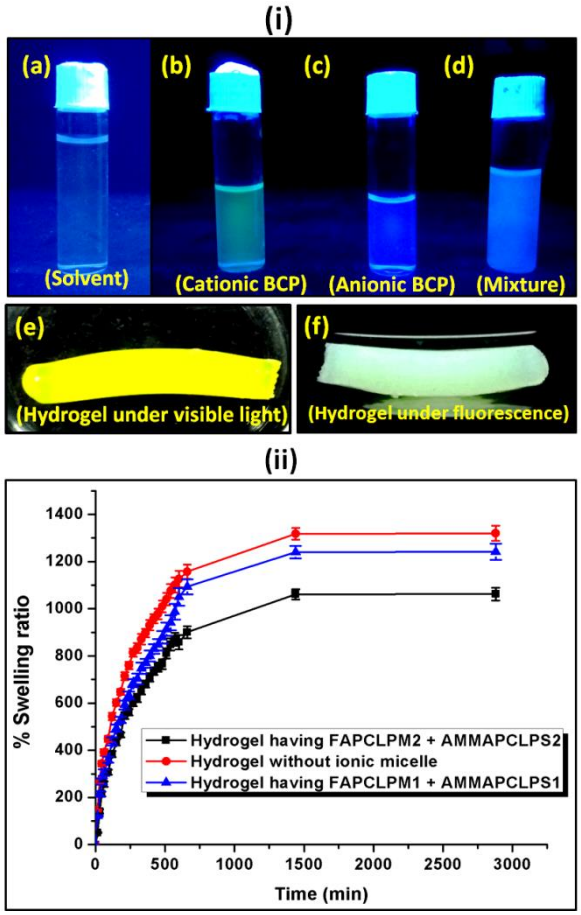

Figure 7 (i) Fluorescent images of the **(a)** solvent (control), **(b)** $FAPCL_{70}$-*b*-$PMTAC_{48}$ micelle, **(c)** $AMMAPCL_{70}$–*b*-PSS_{48} micelle, **(d)** charge neutral mixture of $FAPCL_{70}$-*b*-$PMTAC_{48}$ and $AMMAPCL_{70}$–*b*-PSS_{48}, **(e)** fluorescent hydrogel under visible light, **(f)** fluorescent hydrogel under fluorescence lamp. **(ii)** % Swelling ratio of the prepared hydrogel at pH = 7.4.

The data showed that the incorporation of BCPs of specific block length can provide a higher extent of elongation and modulus compared to the non-modified hydrogel sample. Incorporation of $FAPCL_{70}$-*b*-$PMTAC_{48}$ + AMMA PCL_{70}–*b*-PSS_{48} into the hydrogel provides a (700 ± 10) % ($p < 0.05$) elongation before break as compared to the non-modified hydrogel ((430 ± 10) % elongation before break). This might be due to the presence of elastic ionic interactions between the oppositely charged BCPs[47]. Interestingly, it was observed that the hydrogel with $FAPCL_{70}$-*b*-$PMTAC_{97}$ + AMMA PCL_{70}–*b*-PSS_{97} showed a comparatively lower level of elongation (492 ± 10) % ($p > 0.05$) before break but showed a higher modulus. This result can be explained by considering the transparency result. From the image it is clearly observed that the presence of $FAPCL_{70}$-*b*-$PMTAC_{97}$ + AMMA PCL70–*b*-PSS_{97} provides poor transparency that means generation of higher ionic interaction between the BCPs which leads to large ionic cluster formation. This provides a greater stiffness to the $FAPCL_{70}$-*b*-$PMTAC_{97}$ + AMMA PCL_{70}–*b*-PSS_{97} hydrogel, as compared to the $FAPCL_{70}$-*b*-$PMTAC_{48}$ + AMMA PCL_{70}–*b*-PSS_{48} filled hydrogel. The tensile images of the sample are mentioned in Figure 8c which clearly make a sense about the extent of the elongation of the prepared hydrogels.

Study of the self-healing property of the hydrogel:

In our study we observed the self-healing ability of the BCP ($FAPCL_{70}$-*b*-$PMTAC_{48}$ + AMMA PCL_{70}–*b*-PSS_{48}) incorporated hydrogel at pH = 7.4 (physiological pH) adopting the "scratch and heal" method. For this, we made a notch over the hydrogel surface having a depth of approximately 0.5 mm using a sharp knife. The image of the notched hydrogel sample is represented in Figure 8d(i). After that PBS buffer solution of pH = 7.4 was sprayed over it and kept for 30 minutes at this condition. After that the image of the healed hydrogel sample was again obtained from optical microscope and the image is represented in Figure 8d(ii). Tensile testing of the healed hydrogel was performed to examine the retention of the mechanical properties of the hydrogel after healing. From the tensile testing results (Figure 8e) it was observed that after being healed, the mechanical properties of the hydrogel were almost similar to the uncut hydrogel sample. The healed hydrogel showed a (550 ± 10) % elongation (Tensile strength = 0.19 ± 0.01 MPa), whereas the uncut hydrogel showed a (700 ± 10) % elongation before break (0.32 ± 0.01MPa). The probable reason for the self-healing can be explained by considering the ionic interaction phenomenon. In this case the presence of the oppositely charged BCPs played a role behind the self-healing process. When the buffer solution of pH = 7.4 was sprayed over the cut, the polymeric segments become swollen resulting in close contact of the cationic (containing $-N(CH_3)_3^+$) and the anionic (containing $-SO_3^-$) BCP. Due to the formation of the elastic ionic interaction between the two segments of the hydrogel, after the cut, the hydrogel surface became healed.

DMA analysis:

The ionic interaction induced self-healing in the fluorescent hydrogel system was further studied by the creep and stress relaxation experiments.

Creep Study:

Creep or cold flow of the solid material describes the deformation of the material under a constant stress. The rate of deformation depends on the amount of applied load and exposer time of the load. Creep in the hydrogel occurs due to the viscoelastic nature of it. In our case both the as prepared ionic hydrogel and the self-healed hydrogel was subjected to a step constant stress of 0.1 MPa and the corresponding viscoelastic creep of the hydrogel was recorded. The response from the hydrogel (stress-strain curve) was modelled by using Kelvin-Voigt model as[48]-

$$J(t) = J_0 + \sum_{i=1}^{n} J_i \left[1 - e^{-t/\tau_i}\right]$$

where, $J(t)$ and J_0 are the creep compliance after time t and instant compliance respectively. J_0 and τ_i are constant. From the Figure 8f, it was observed that compared to the as prepared hydrogel, the self-healed hydrogel responded faster to the applied stress. From the obtained result it can be said that due to the consecutive cut and healing process, an obvious loss of covalent bond (crosslinking by MBA) occurred in case of the self-healed hydrogel. As a result, a high amount of primary creep or transient creep was observed in the case of self-healed hydrogel as compared to as prepared hydrogel. It was observed that the rate of achieving the secondary creep or "steady-state-creep" was higher in case of self-healed gel as compared to as prepared hydrogel. The data thus indicate that the only factor that resists the applied stress was the ionic interaction which acted between the ionic BCP micelle inside the hydrogel. This indeed supports the concept of ionic interactions as the main driver of self-healing[49]. Whereas, in the as prepared hydrogel, due to the presence of both covalent bonds and ionic interactions, the resistance against the applied stress was high. As a result achievement of the secondary creep stage was delayed. Although, both hydrogels showed a comparable creep compliance value (Figure S6). It was observed that both hydrogels had not experienced any tertiary stage creep in the presence of 0.1 MPa stress for a time period of 1200 sec. An immediate drop of strain was observed after the withdrawal of the stress. As a result, a gradual recovery of the residual strain was witnessed. The extent of the immediate drop in strain was slightly increased in the case of the as prepared hydrogel compared to the self-healed hydrogel and this difference was ascribed to the synergistic contribution of both the covalent crosslink and ionic crosslinks towards the elasticity.

Stress relaxation study:

Stress relaxation can be explained as the decrease in stress at constant strain condition. In our hydrogel system, both the hydrogels (as prepared and self-healed) passed through a constant strain of 0.02% @ 25°C. From the Figure 8g, it can be observed that the rate of relaxation of stress was faster in case of the as prepared hydrogel compared to the self-healed one. Maxwell modelled the stress relaxation as-

$$E(t) = \sum_{i=1}^{n} E_i \, e^{-t/\tau_i}$$

where, $E(t)$ is the relaxation modulus at time (t) and E_i and τ_i are the constants. SAs observed in the creep experiment from the stress relaxation curve (stress-time curve) showed that the response of the as prepared hydrogel was rapid compared to the self-healed hydrogel (relaxation of stress) after removal of the applied strain. This again proves the higher elasticity of the as prepared hydrogel due to the combined effect of covalent crosslinks and ionic interactions[50]. Whereas, in the case of self-healed gel the relaxation only occurred due to the presence of ionic interaction which also supports the concept of ionic interaction based healing.

***In-vitro* cell cytotoxicity assay:**

An *in-vitro* cell viability study was carried out to determine the cell cytotoxicity of the synthesized hydrogel. Charged polymers in solution or as block copolymers in micellar dispersion are often toxic if they are allowed to disrupt cell membranes. To estimate the cell cytotoxicity of the prepared hydrogel a MTT colorimetric assay test was carried out using NIH 3T3 fibroblast cells as the test cell line. From the Figure 9 it was observed that the hydrogels containing the BCP of different ionic block lengths showed good cell proliferation compared to the control sample. It is reported that the cell proliferation in some way depends on the surface hydrophilicity and the micro roughness of the surface[51]. As shown in Figure S5(b) on formation of the ionic BCPs the WCA value reduced from 78° (homo PCL) to 32° for cationic BCP and 36° for the anionic BCP. Furthermore upon mixing of the two ionic BCPs at almost equal charge ratio the WCA value of decreased to 20° and a rough surface was created, as shown in FESEM and AFM analysis. Both of these factors and the charge state of the hydrogel are expected to provide a surface that is favourable for cell proliferation. The extent of cytotoxicity can be measured by measuring the O.D. value of the formed purple formazan salt at 590 nm. The absorbance result of the cytotoxicity assay is summarized in Figure 9d. Student's t-test was carried out to compare the statistical significance of the test samples (hydrogel with FAPCL$_{70}$-b-PMTAC$_{48}$ + AMMA PCL$_{70}$–b-PSS$_{48}$ (Sample 1) and FAPCL$_{70}$-*b*-PMTAC$_{97}$ + AMMA PCL$_{70}$–*b*-PSS$_{97}$ (Sample 2)) against control (only polyacrylamide hydrogel) and it was found that the $p > 0.05$ which signifies that there is no significant difference in the cell proliferation over the test sample as compared to the control one. So it can be concluded that in presence of the test sample there was no cell death. This indicates that the prepared hydrogels are non-toxic in nature compared to a conventional polyacrylamide gel.

Journal Name

ARTICLE

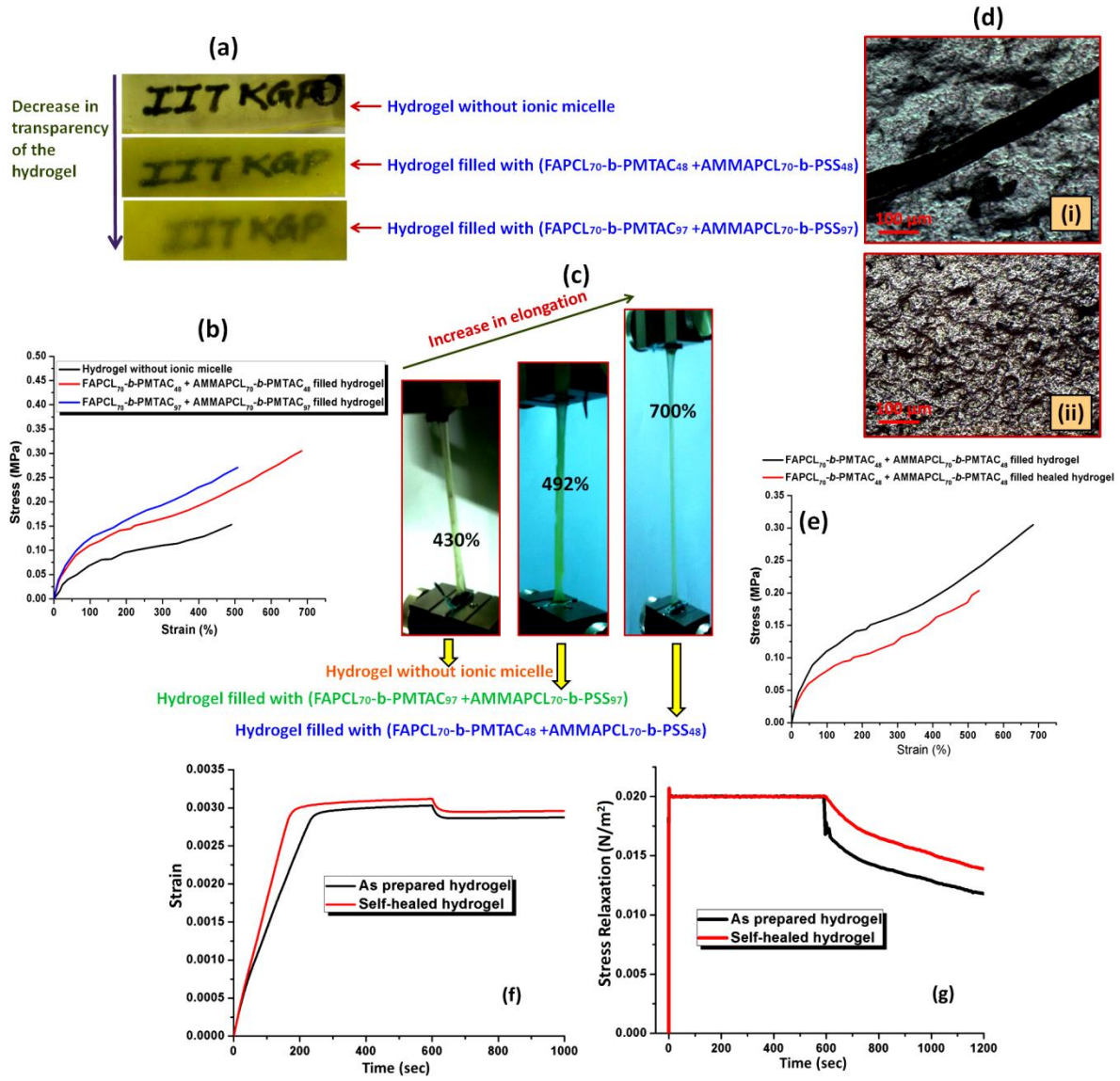

Figure 8 (a) Variation of the transparency of the hydrogel upon incorporation of micelle of different block lengths, (b) tensile strength measurement, (c) picture of extent of elongation of hydrogel upon incorporation of micelle of different block length, (d) images of (i) notched and (ii) healed hydrogel, (e) tensile test of as prepared and healed hydrogel, (f) comparative creep study of the hydrogels under a constant stress of 0.1 MPa @ 25°C, (g) comparative stress relaxation study of the hydrogels under a constant strain of 0.02% @ 25°C.

Journal Name

ARTICLE

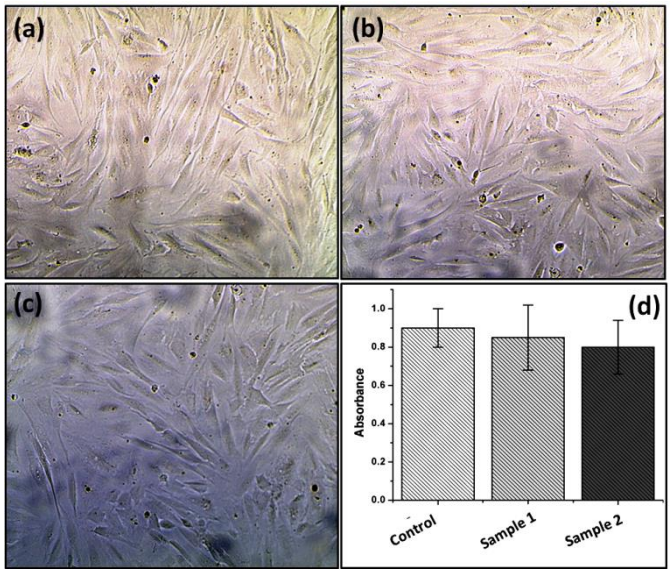

Figure 9: *In-vitro* cell cytotoxicity assay of (a) control sample (only polyacrylamide hydrogel), (b) $FAPCL_{70}$-b-$PMTAC_{48}$ + AMMA PCL_{70}–b-PSS_{48} filled hydrogel and (c) $FAPCL_{70}$-b-$PMTAC_{97}$ + AMMA PCL_{70}–b-PSS_{97} filled hydrogel against NIH 3T3 fibroblast cell and (d) respective absorbance values.

Conclusions

PCL based fluorescent labelled cationic (FA tagged) and anionic (AMMA tagged) block copolymers were successfully prepared using consecutive ROP of ε-caprolactone and xanthate mediated RAFT polymerization. The BCPs are able to form micelles in a 1 : 4 (volume ratio) DMF:water mixture with core shell morphologies. The formed morphology was evaluated by using FESEM, HRTEM and AFM analyses. The size distribution and hydrodynamic diameter of the formed micelle were determined using DLS analysis. Water contact angle analysis also supports the formation of BCPs by showing a reduced water contact angle value as compared to PCL. After that the oppositely charged BCPs were incorporated into a poly(acrylamide) based hydrogel. Importantly, this material showed fluorescent emission under visible light and fluorescent light. Along with the fluorescent phenomenon the modified hydrogel was able to self-heal at pH = 7.4. MTT assay experiment revealed that the synthesized fluorescent active hydrogels are non-toxic in nature. This type of fluorescence active self-healable, mechanically strong and non-toxic hydrogels may be a potentially smart material in the field of tissue engineering and sensing applications in near future.

Conflicts of interest

There are no conflicts to declare.

Acknowledgements

Funding for Mr. Sovan Lal Banerjee's fellowship was kindly provided by IIT Kharagpur.

Notes and references

1. Wichterle, O.; Lim, D., Hydrophilic Gels for Biological Use. Nature 1960, 185 (4706), 117-118.
2. Lee, K. Y.; Mooney, D. J., Hydrogels for Tissue Engineering. Chemical reviews 2001, 101 (7), 1869-1880.
3. Dai, H.; Chen, Q.; Qin, H.; Guan, Y.; Shen, D.; Hua, Y.; Tang, Y.; Xu, J., A Temperature-Responsive Copolymer Hydrogel in Controlled Drug Delivery. Macromolecules 2006, 39 (19), 6584-6589.
4. Luo, Y.; Shoichet, M. S., A Photolabile Hydrogel for Guided Three-Dimensional Cell Growth and Migration. Nature materials 2004, 3 (4), 249.
5. Hasan, A.; Paul, A.; Vrana, N. E.; Zhao, X.; Memic, A.; Hwang, Y.-S.; Dokmeci, M. R.; Khademhosseini, A., Microfluidic Techniques for Development of 3D Vascularized Tissue. Biomaterials 2014, 35 (26), 7308-7325.
6. Song, S. J.; Choi, J.; Park, Y. D.; Lee, J. J.; Hong, S. Y.; Sun, K., A Three-Dimensional Bioprinting System for Use With a Hydrogel-Based Biomaterial and Printing Parameter Characterization. Artificial organs 2010, 34 (11), 1044-1048.
7. Hoffman, A. S., Hydrogels for biomedical applications. Advanced drug delivery reviews 2012, 64, 18-23.
8. Zhang, X.; Pint, C. L.; Lee, M. H.; Schubert, B. E.; Jamshidi, A.; Takei, K.; Ko, H.; Gillies, A.; Bardhan, R.; Urban, J. J., Optically-and thermally-responsive Programmable Materials based on Carbon Nanotube-hydrogel Polymer Composites. Nano letters 2011, 11 (8), 3239-3244.
9. Heo, Y. J.; Shibata, H.; Okitsu, T.; Kawanishi, T.; Takeuchi, S., Long-term in vivo Glucose Monitoring using Fluorescent Hydrogel Fibers. Proceedings of the National Academy of Sciences 2011, 108 (33), 13399-13403.
10. Suri, J. T.; Cordes, D. B.; Cappuccio, F. E.; Wessling, R. A.; Singaram, B., Continuous glucose sensing with a fluorescent thin-film hydrogel. Angewandte Chemie International Edition 2003, 42 (47), 5857-5859.
11. Gong, Y.; Gao, M.; Wang, D.; Möhwald, H., Incorporating Fluorescent CdTe Nanocrystals into a Hydrogel via Hydrogen Bonding: Toward Fluorescent Microspheres with Temperature-responsive Properties. Chemistry of materials 2005, 17 (10), 2648-2653.
12. HyeanáKim, B., An insulin-sensing sugar-based fluorescent hydrogel. Chemical communications 2006, (17), 1842-1844.
13. Artzi, N.; Oliva, N.; Puron, C.; Shitreet, S.; Artzi, S.; Bon Ramos, A.; Groothuis, A.; Sahagian, G.; Edelman, E. R., In Vivo and in Vitro Tracking of Erosion in Biodegradable materials Using non-invasive Fluorescence Imaging. Nature materials 2011, 10 (9), 704.

14. Wang, W.; Liu, J.; Li, C.; Zhang, J.; Liu, J.; Dong, A.; Kong, D., Real-time and Non-invasive Fluorescence Tracking of In Vivo Degradation of the Thermosensitive PEGlyated Polyester Hydrogel. Journal of Materials Chemistry B 2014, 2 (26), 4185-4192.
15. Dong, Y.; Jin, G.; Ji, C.; He, R.; Lin, M.; Zhao, X.; Li, A.; Lu, T. J.; Xu, F., Non-invasive tracking of Hydrogel Degradation Using Upconversion Nanoparticles. Acta Biomaterialia 2017, 55, 410-419.
16. Shkand, T. V.; Chizh, M. O.; Sleta, I. V.; Sandomirsky, B. P.; Tatarets, A. L.; Patsenker, L. D., Assessment of Alginate Hydrogel Degradation in Biological Tissue Using Viscosity-sensitive Fluorescent Dyes. Methods and Applications in Fluorescence 2016, 4 (4), 044002.
17. Ma, X.; Sun, X.; Hargrove, D.; Chen, J.; Song, D.; Dong, Q.; Lu, X.; Fan, T.-H.; Fu, Y.; Lei, Y., A Biocompatible and Biodegradable Protein Hydrogel with Green and Red Autofluorescence: preparation, Characterization and In vivo Biodegradation Tracking and Modeling. Scientific reports 2016, 6.
18. Mako, T.; Levine, M., Synthesis of a Fluorescent Conjugated Polymer in the Undergraduate Organic Teaching Laboratory. Journal of Chemical Education 2013, 90 (10), 1376-1379.
19. Ribeiro, A. S.; Mortimer, R. J., Conjugated Conducting Polymers with Electrochromic and Fluorescent Properties. In Electrochemistry, 2015; pp 21-49.
20. Tovmachenko, O. G.; Graf, C.; van den Heuvel, D. J.; van Blaaderen, A.; Gerritsen, H. C., Fluorescence Enhancement by Metal-core/silica-shell Nanoparticles. Advanced materials 2006, 18 (1), 91-95.
21. Liu, J.; Hurt, R. H., Ion Release Kinetics and Particle Persistence in Aqueous Nano-silver Colloids. Environ. Sci. Technol 2010, 44 (6), 2169-2175.
22. Zhang, X.; Wang, S.; Xu, L.; Feng, L.; Ji, Y.; Tao, L.; Wei, Y.; Biocompatible polydopamine fluorescent organic nanoparticles: facile preparation and cell imaging. Nanoscale 2012, 4(18), 5581-5584.
23. Loo, A. H.; Sofer, Z.; Bouša, D.; Ulbrich, P.; Bonanni, A.; Pumera, M., Carboxylic Carbon Quantum Dots as a Fluorescent Sensing Platform for DNA Detection. ACS applied materials & interfaces 2016, 8 (3), 1951-1957.
24. Chowdhury, D.; Gogoi, N.; Majumdar, G., Fluorescent carbon dots obtained from chitosan gel. RSC Advances 2012, 2 (32), 12156-12159.
25. Cayuela, A.; Soriano, M. L.; Kennedy, S. R.; Steed, J.; Valcárcel, M., Fluorescent Carbon Quantum Dot Hydrogels for Direct Determination of Silver Ions. Talanta 2016, 151, 100-105.
26. Neyfakh, A. A., Use of Fluorescent Dyes as Molecular Probes for the Study of Multidrug Resistance. Experimental cell research 1988, 174 (1), 168-176.
27. Zhang, X.; Wang, K.; Liu, M.; Zhang, X.; Tao, L.; Chen, Y.; Wei, Y., Polymeric AIE-based nanoprobes for biomedical applications: recent advances and perspectives. Nanoscale, 2015, 7(27), 11486-11508.
28. Swift, T.; Swanson, L.; Geoghegan, M.; Rimmer, S., The pH-responsive Behaviour of Poly(acrylic acid) in Aqueous Solution is Dependent on Molar Mass. Soft Matter 2016, 12 (9), 2542-2549.
29. Ruiz-Pérez, L.; Pryke, A.; Sommer, M.; Battaglia, G.; Soutar, I.; Swanson, L.; Geoghegan, M., Conformation of Poly(methacrylic acid) Chains in Dilute Aqueous Solution. Macromolecules 2008, 41 (6), 2203-2211.
30. Swift, T.; Swanson, L.; Rimmer, S., Poly(acrylic acid) Interpolymer Complexation: use of a Fluorescence Time Resolved Anisotropy as a Poly(acrylamide) Probe. RSC Advances 2014, 4 (101), 57991-57995.
31. Heyward, J. J.; Ghiggino, K. P., Fluorescence Polarization study of the poly(acrylic acid)/poly(ethylene oxide) Interpolymer Complex in Aqueous Solution. Macromolecules 1989, 22 (3), 1159-1165.
32. Swift, T.; Lapworth, J.; Swindells, K.; Swanson, L.; Rimmer, S., pH Responsive Highly Branched poly(N-isopropylacrylamide) with Trihistidine or Acid Chain Ends. RSC Advances 2016, 6 (75), 71345-71350.
33. Swift, T.; Paul, N.; Swanson, L.; Katsikogianni, M.; Rimmer, S., Förster Resonance Energy Transfer Across Interpolymer Complexes of Poly(acrylic acid) and Poly(acrylamide). Polymer.
34. Banerjee, S. L.; Khamrai, M.; Kundu, P.; Singha, N. K., Synthesis of a Self-healable and pH Responsive Hydrogel Based on an Ionic Polymer/clay Nanocomposite. RSC Advances 2016, 6 (85), 81654-81665.
35. Habault, D.; Zhang, H.; Zhao, Y., Light-triggered Self-healing and Shape-memory Polymers. Chemical Society Reviews 2013, 42 (17), 7244-7256.
36. Liu, Y.-L.; Chuo, T.-W., Self-healing polymers based on thermally reversible Diels–Alder chemistry. Polymer Chemistry 2013, 4 (7), 2194-2205.
37. Gao, H.; Wang, N.; Hu, X.; Nan, W.; Han, Y.; Liu, W., Double Hydrogen-Bonding pH-Sensitive Hydrogels Retaining High-Strengths Over a Wide pH Range. Macromolecular rapid communications 2013, 34 (1), 63-68.
38. Li, C.; Shi, G., Functional gels based on chemically modified graphenes. Advanced materials 2014, 26 (24), 3992-4012.
39. Foster, J. A.; Parker, R. M.; Belenguer, A. M.; Kishi, N.; Sutton, S.; Abell, C.; Nitschke, J. R., Differentially addressable cavities within metal–organic cage-cross-linked polymeric hydrogels. Journal of the American Chemical Society 2015, 137 (30), 9722-9729.
40. Kuo, S. W.; Huang, C. F.; Lu, C. H.; Lin, H. M.; Jeong, K. U.; Chang, F. C., Syntheses and Specific Interactions of Poly (ε-caprolactone)-block-poly (vinyl phenol) Copolymers Obtained via a Combination of Ring-Opening and Atom-Transfer Radical Polymerizations. Macromolecular Chemistry and Physics 2006, 207 (21).
41. Patel, V. K.; Mishra, A. K.; Vishwakarma, N. K.; Biswas, C. S.; Ray, B., (S)-2-(Ethyl propionate)-(O-ethyl xanthate) and (S)-2-(Ethyl isobutyrate)-(O-ethyl xanthate)-mediated RAFT polymerization of N-vinylpyrrolidone. Polymer bulletin 2010, 65 (2), 97-110.
42. Swift, T.; Hoskins, R.; Telford, R.; Plenderleith, R.; Pownall, D.; Rimmer, S., Analysis Using Size Exclusion Chromatography of poly(N-isopropyl acrylamide) using Methanol as an Eluent. Journal of Chromatography A.
43. Gupta, K. K.; Kundan, A.; Mishra, P. K.; Srivastava, P.; Mohanty, S.; Singh, N. K.; Mishra, A.; Maiti, P., Polycaprolactone composites with TiO 2 for potential nanobiomaterials: tunable properties using different phases. Physical Chemistry Chemical Physics 2012, 14 (37), 12844-12853.
44. Owen, S. C.; Chan, D. P.; Shoichet, M. S., Polymeric Micelle Stability. Nano Today 2012, 7 (1), 53-65.
45. Riess, G., Micellization of Block Copolymers. Progress in Polymer Science 2003, 28 (7), 1107-1170.
46. Zhai, S.; Ma, Y.; Chen, Y.; Li, D.; Cao, J.; Liu, Y.; Cai, M.; Xie, X.; Chen, Y.; Luo, X., Synthesis of an Amphiphilic Block Copolymer Containing Zwitterionic Sulfobetaine as a Novel pH-sensitive Drug Carrier. Polymer Chemistry 2014, 5 (4), 1285-1297.
47. Sun, T. L.; Kurokawa, T.; Kuroda, S.; Ihsan, A. B.; Akasaki, T.; Sato, K.; Haque, M. A.; Nakajima, T.; Gong, J. P., Physical hydrogels Composed of Polyampholytes Demonstrate High Toughness and Viscoelasticity. Nature materials 2013, 12 (10), 932-937.

48. Shaw, M. T.; MacKnight, W. J. Introduction to Polymer Viscoelasticity, 3rd ed.; John Wiley & Sons, Inc., Hoboken, New Jersey 2005; Chapter 2, p 51.
49. Karobi, S. N., Sun, T. L., Kurokawa, T., Luo, F., Nakajima, T., Nonoyama, T., Gong, J. P.. Creep Behavior and Delayed Fracture of Tough Polyampholyte Hydrogels by Tensile Test. Macromolecules 2016, 49(15), 5630-5636.
50. Zhao, X., Huebsch, N., Mooney, D. J., Suo, Z.. Stress-relaxation behavior in gels with ionic and covalent crosslinks. Journal of Applied Physics 2010, 107(6), 063509.
51. Yuan, S., Xiong, G., Wang, X., Zhang, S., & Choong, C.. Surface modification of polycaprolactone substrates using collagen-conjugated poly (methacrylic acid) brushes for the regulation of cell proliferation and endothelialisation. Journal of Materials Chemistry 2012, 22(26), 13039-13049.